Journal of Engineering Mathematics **30:** 445–457, 1996.

An asymptotic analysis of small holes in thin fluid layers

S. K. WILSON AND B. R. DUFFY
Department of Mathematics, University of Strathclyde, Livingstone Tower, 26 Richmond Street, Glasgow G1 1XH

Received 17 February 1995; accepted in revised form 2 August 1995

Abstract. In this paper we obtain the description of axisymmetric equilibrium holes in thin fluid layers lying on a horizontal substrate under the influence of surface tension and gravity effects in the asymptotic limit when the radius of the hole is small. For values of the contact angle between the fluid and the substrate not equal to π we demonstrate that James' (*J. Fluid Mech.* **63**, 657-664 (1974)) solution for the meniscus surrounding a narrow cylindrical rod dipped into a bath of fluid also provides the correct asymptotic solution to the present problem. In the case when the contact angle is equal to π we obtain the asymptotic solution for the first time. In both cases we obtain asymptotic expressions for the radius of the hole at the substrate and the thickness of the layer far from the hole. The correctness of these expressions is confirmed by comparison with numerical solutions to the full problem. In the light of the present study we are able to highlight shortcomings in previous studies and, in particular, show that their predictions for the thickness of the layer are correct only at leading order in the limit of small holes.

1. Introduction

In the coating industry it is of considerable practical importance to understand when a fluid layer applied to a substrate can contain holes which leave parts of the substrate uncoated, and if holes can exist then whether or not they will close up during the coating process.

The pioneering theoretical and experimental work of Taylor and Michael [1] showed that a fluid layer lying on a horizontal plane under the influence of surface tension and gravity effects has a unique axisymmetric equilibrium hole configuration provided that the layer is sufficiently thin, and that if the layer is too thick then no such hole can exist. By considering the energy of this equilibrium configuration Taylor and Michael [1] showed that all these holes are unstable, and conjectured that non-equilibrium holes with radius smaller than that of this unstable equilibrium hole would close while those with larger radius would open. To test their hypothesis Taylor and Michael [1] conducted a series of experiments in which holes were made in a horizontal layer of mercury standing on a glass disc with a series of cylindrical probes of different radii. All the holes either opened or closed, and the division between the two kinds of behaviour was in good agreement with the theoretically calculated critical radius. Recently Wilson and Terrill [2] have confirmed these conclusions analytically for holes in thin fluid layers in the limit of quasi-steady motion in which the dynamics are governed entirely by those of the moving contact line. An important conclusion from both these studies is that knowledge of the radius of the equilibrium hole configuration is of considerable practical importance since, at least in the quasi-static limit, it demarcates holes that open from holes that close.

In general the equilibrium shape of the free surface of the fluid (which satisfies the well-known Young-Laplace equation) and hence the relationship between the hole radius, the

contact angle between the fluid and the substrate and the thickness of the layer far from the hole can only be determined numerically. However, analytical progress is possible in two limiting cases, namely when the hole is large and when the hole is small. When the hole radius is large, azimuthal curvature effects become insignificant and the limiting problem is simply that of a planar hole, which can be solved exactly (see, for example, Lamb (3, §127)). However, when the hole radius is small, the situation is less clear. Sykes [4] presented an ad hoc treatment of the problem which yielded an analytical prediction for the layer thickness which the present work shows is correct only at leading order. More recently, Sharma [5] presented an asymptotic analysis of the problem in this limit. Unfortunately his analysis of the solution as the free surface becomes horizontal is flawed, with the consequence that his analytical prediction for the layer thickness is also correct only at leading order. However, both these authors apparently failed to realise that the correct asymptotic solution had essentially been obtained almost twenty years earlier by James [6] in the context of the formally equivalent problem of the meniscus surrounding a narrow cylindrical rod dipped into a bath of fluid.

The aim of the present paper is to provide the solution to the hole problem in the asymptotic limit when the radius of the hole is small. For values of the contact angle not equal to π we shall demonstrate that James' [6] solution for the meniscus surrounding a narrow cylindrical rod, which was subsequently extended to higher orders by Lo [7], also provides the correct asymptotic solution to the present problem. When the contact angle is equal to π we shall obtain the asymptotic solution for the first time. In both cases the resulting predictions for the radius of the hole at the substrate and the layer thickness far from the hole will be verified by comparison with numerical solutions to the full problem.

2. Problem formulation

Consider a layer of fluid with constant density ρ lying on a solid horizontal planar substrate in equilibrium under the influence of constant surface tension σ and acceleration due to gravity g. We non-dimensionalise the problem using the characteristic capillary length, $l_c = (\sigma/\rho g)^{1/2}$. We wish to investigate the situation in which the fluid layer has thickness $\hat{H}$ far from a single axisymmetric hole with minimum radius R_m and the fluid makes a (static) contact angle $\theta \in (0, \pi]$ with the substrate. To describe the situation we employ cylindrical polar coordinates (R, Z), with Z measured vertically upwards, whose origin is chosen to be at the centre of the hole.

As Huh and Scriven [8] were the first to point out, a considerable simplification of the analysis can be achieved if we treat R_m rather than $\hat{H}$ as the independent variable, because then for each value of R_m there is a single "universal" solution to the governing equation from which the value of $\hat{H}$ can simply be read off for *all* values of $\theta \in (0, \pi]$. In contrast, if $\hat{H}$ is taken as the independent variable then a new solution to the governing equation has to be calculated for *each* value of $\theta \in (0, \pi]$.

If we denote the position of the free surface of the fluid by $R = R(Z)$ and choose the origin of the coordinate system so that $R = R_m$ at $Z = 0$ then the function $R(Z)$ satisfies the classical Young-Laplace equation (representing the static balance between surface tension and gravity effects) which can be written in the form

$$R_{ZZ} - \frac{1}{R}(1 + R_Z^2) = (H_1 - Z)(1 + R_Z^2)^{\frac{3}{2}}. \tag{1}$$

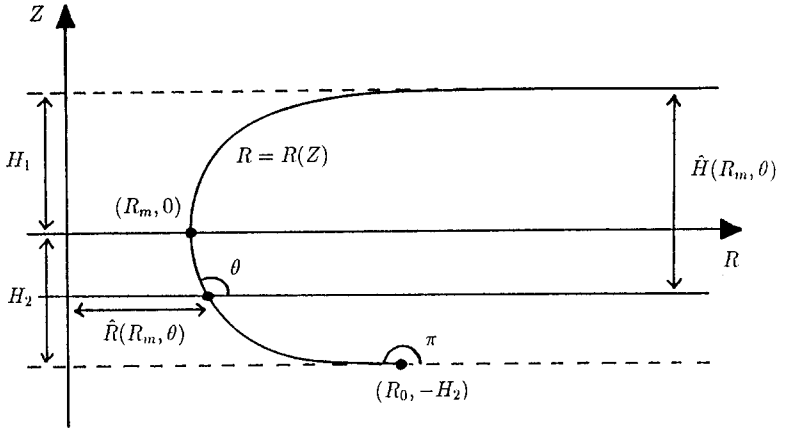

Fig. 1. The geometry of the problem

Equation (1) has a unique solution that, in addition to the condition

$$R = R_m \quad \text{at} \quad Z = 0, \tag{2}$$

satisfies

$$R, R_Z \to \infty \quad \text{as} \quad Z \to H_1^-, \tag{3}$$

$$R = R_0 \quad \text{at} \quad Z = -H_2, \tag{4}$$

$$R_Z \to -\infty \quad \text{as} \quad Z \to -H_2^+, \tag{5}$$

as shown in Figure 1. The values of $H_1 = H_1(R_m)$, $H_2 = H_2(R_m)$ and $R_0 = R_0(R_m)$ are all determined as part of the solution and we denote the maximum width of the universal curve by $H = H(R_m) = H_1 + H_2$.

In just the same way as O'Brien [9] describes for the related problem of a sessile drop, the solution for an axisymmetric hole with contact angle $\theta \in (0, \pi]$ is obtained by truncating the curve $R = R(Z)$ at the point where $R_Z = \cot\theta$, corresponding to a hole with radius at the substrate $\hat{R} = \hat{R}(R_m, \theta)$ and layer thickness far from the hole $\hat{H} = \hat{H}(R_m, \theta)$. This procedure is illustrated in Fig. 1. Note that since the angle between the tangent to the universal curve and the R-axis increases monotonically from 0^+ at $Z = H_1^-$ to π at $Z = -H_2$ this truncation can always be performed uniquely. If $\theta \in (0, \pi/2)$ then the truncated profile corresponds to a hole with minimum radius $\hat{R}$ at the substrate $Z = H_1 - \hat{H} > 0$, while if $\theta \in (\pi/2, \pi]$ then it corresponds to a hole with minimum radius R_m at $Z = 0$ and radius $\hat{R} > R_m$ at the substrate $Z = H_1 - \hat{H} < 0$. We note that by construction $R_m = \hat{R}(R_m, \pi/2)$, $R_0 = \hat{R}(R_m, \pi)$, $H_1 = \hat{H}(R_m, \pi/2)$ and $H = \hat{H}(R_m, \pi)$ and that $\hat{R} = \hat{R}(R_m, \theta) \to \infty$ and $\hat{H} = \hat{H}(R_m, \theta) \to 0$ as $\theta \to 0$. Figure 2 gives typical numerically calculated curves $R = R(Z)$ for a range of values of R_m which complement the corresponding curves given by Huh and Scriven [8, Fig. 2]. Details of the numerical techniques used to obtain the curves shown in Figure 2 are described in section 4.

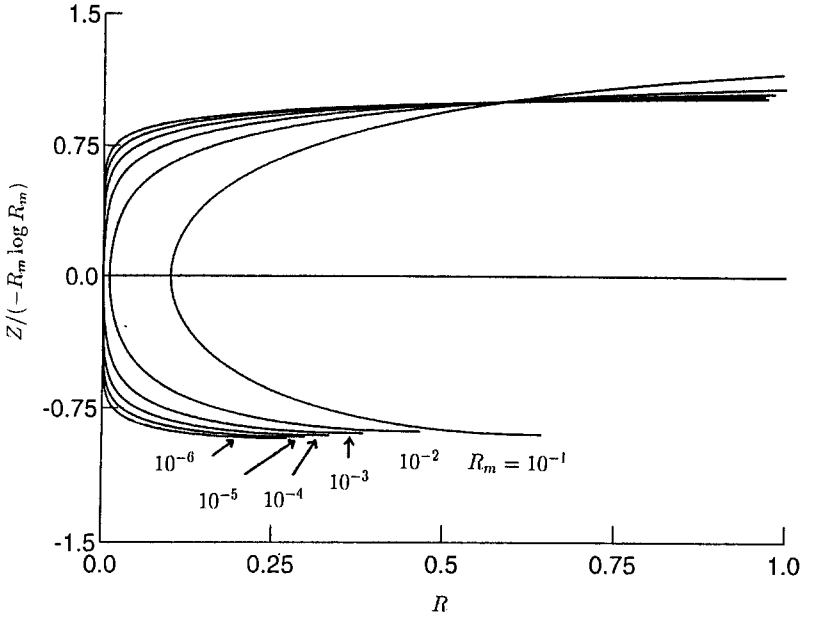

Fig. 2. Numerically calculated curves $R = R(Z)$ for $R_m = 10^{-1}, 10^{-2}, \ldots, 10^{-6}$. Note that in order to show all the curves on the same axes Z has been scaled with $-R_m \log R_m$.

3. Asymptotic solution for small holes

Numerical solutions of the full problem indicate that $\hat{H}$ is a monotonically increasing function of $R_m > 0$ which satisfies

$$0 < \hat{H} \leq 2\sin(\theta/2), \tag{6}$$

the upper bound being obtained in the limit $R_m \to \infty$. We seek the asymptotic solution to the present problem, and in particular expressions for the functions $\hat{R}(R_m, \theta)$ and $\hat{H}(R_m, \theta)$, in the limit of small holes $R_m \to 0$.

3.1. Region 1 : Near $Z = 0$

Near $Z = 0$ both R and Z are of the same order as R_m, and so we introduce appropriately rescaled variables r_1 and z_1 such that $R = R_m r_1$ and $Z = R_m z_1$, and write $H_1 = R_m h_1$, $H_2 = R_m h_2$ and $H = R_m h$. In terms of these new variables equation (1) becomes

$$r_{1z_1z_1} - \frac{1}{r_1}(1 + r_{1z_1}^2) = {R_m}^2(h_1 - z_1)(1 + r_{1z_1}^2)^{\frac{3}{2}}, \tag{7}$$

and so at leading order in R_m we obtain the equation

$$r_{1z_1z_1} - \frac{1}{r_1}(1 + r_{1z_1}^2) = 0, \tag{8}$$

subject to the boundary conditions

$$r_1(0) = 1, \quad r_{1z_1}(0) = 0. \tag{9}$$

Equation (8) is simply the Young-Laplace equation in the absence of gravity and can be readily solved subject to the boundary conditions (9) to yield

$$r_1(z_1) = \cosh z_1. \tag{10}$$

3.2. Region 2 : Near $Z = H_1$

Near the horizontal asymptote at $Z = H_1$ gravity effects become significant and equation (8) no longer describes the leading order behaviour correctly. In order to rectify this we introduce rescaled variables r_2 and z_2 such that $r_1 = \bar{R} r_2$ and $\delta_2 z_2 = h_1 - z_1$, where the unknown scalings $\bar{R}$ and δ_2 satisfy $\bar{R} \gg \delta_2$ and $\delta_2 \ll h_1$. Gravity effects will balance surface tension effects at leading order only if we choose $\bar{R} = 1/R_m$, in which case the leading order version of equation (1) is given by

$$r_{2z_2z_2} - \frac{1}{r_2} r_{2z_2}^2 = -z_2 r_{2z_2}^3, \tag{11}$$

subject to the boundary condition

$$r_2 \to \infty \quad \text{as} \quad z_2 \to 0. \tag{12}$$

Writing $z_2 = z_2(r_2)$ instead of $r_2 = r_2(z_2)$, equation (11) becomes

$$z_{2r_2r_2} + \frac{1}{r_2} z_{2r_2} = z_2, \tag{13}$$

with solution $z_2 = A_2 I_0(r_2) + B_2 K_0(r_2)$, where $I_0(\cdot)$ and $K_0(\cdot)$ denote Bessel functions of imaginary argument of zeroth order of the first and second kind respectively, and A_2 and B_2 are constants. Since $I_0(r_2) = O({r_2}^{-\frac{1}{2}} e^{r_2})$ and $K_0(r_2) = O({r_2}^{-\frac{1}{2}} e^{-r_2})$ as $r_2 \to \infty$, this solution can satisfy the boundary condition (12) only if $A_2 = 0$, and so

$$z_2(r_2) = B_2 K_0(r_2), \tag{14}$$

where the constant B_2 is as yet undetermined. Since $K_0(r_2) = O(\log r_2)$ as $r_2 \to 0$, we note that $r_2 = O(e^{-z_2})$ as $z_2 \to \infty$.

As an aside we note that this analysis also shows that Taylor and Michael's [1, p.632] assertion that azimuthal curvature effects are insignificant near $Z = H_1$ and hence that $Z = O(e^{-R})$ as $R \to \infty$ (just as in the planar problem) is not justified in the present limit, and that the correct behaviour is in fact $Z = O(R^{-\frac{1}{2}} e^{-R})$ as $R \to \infty$.

3.3. Region 3 : Near $Z = -H_2$

Gravity effects also become significant near $Z = -H_2$, where once again equation (8) fails to describe the leading order behaviour correctly. In this region R is of the same order as R_0 and so we introduce rescaled variables r_3 and z_3 such that $r_1 = R_0 r_3 / R_m$ and $\delta_3 z_3 = h_2 + z_1$, where the unknown scaling δ_3 satisfies $R_0 \gg \delta_3 R_m$ and $\delta_3 \ll h_2$. Gravity effects will balance surface tension effects at leading order only if $2\bar{h} R_0^2 = \delta_3$, where we have defined the unknown scaling $\bar{h}$ such that $h = h_1 + h_2 \sim 2\bar{h}$ as $R_m \to 0$, in which case the leading order version of equation (1) is given by

$$r_{3z_3z_3} - \frac{1}{r_3} r_{3z_3}^2 = -r_{3z_3}^3, \tag{15}$$

subject to the boundary conditions

$$r_3(0) = 1, \quad r_{3z_3} \to -\infty \quad \text{as} \quad z_3 \to 0. \tag{16}$$

Writing $z_3 = z_3(r_3)$ instead of $r_3 = r_3(z_3)$, equation (15) becomes

$$z_{3r_3r_3} + \frac{1}{r_3} z_{3r_3} = 1, \tag{17}$$

with solution

$$z_3 = \frac{1}{4}({r_3}^2 - 1) - \frac{1}{2}\log r_3, \tag{18}$$

satisfying the boundary conditions in equation (16). Note that $r_3 = O(e^{-z_3})$ as $z_3 \to \infty$.

3.4. MATCHING

In the previous three subsections we have obtained the leading order asymptotic solutions for $R(Z)$ near $Z = 0$, $Z = H_1$ and $Z = -H_2$. The solution is completed by ensuring that these solutions match correctly in their regions of common validity.

3.4.1. *Regions 1 and 2*

As $z_1 \to \infty$

$$r_1 \sim \frac{1}{2} e^{z_1}. \tag{19}$$

Since $K_0(R) = -\log R + \log 2 - \gamma + O(R^2 \log R)$, where $\gamma \simeq 0.5772156649$ is Euler's constant, we deduce that as $z_2 \to \infty$

$$r_2 \sim 2e^{-\gamma} e^{-z_2/B_2}. \tag{20}$$

Writing the expressions in equations (19) and (20) in unscaled variables, we see that the solutions will match provided that

$$\frac{R_m}{2} e^{Z/R_m} = 2e^{-\gamma} e^{-(H_1 - Z)/(\delta_2 B_2 R_m)}, \tag{21}$$

i.e. provided that $\delta_2 B_2 = 1$ and

$$H_1 = R_m \log\left(\frac{4e^{-\gamma}}{R_m}\right). \tag{22}$$

3.4.2. *Regions 1 and 3*

As $z_1 \to -\infty$

$$r_1 \sim \frac{1}{2} e^{-z_1}, \tag{23}$$

and as $z_3 \to \infty$

$$r_3 \sim e^{-1/2} e^{-2z_3}. \tag{24}$$

Writing the expressions in equations (23) and (24) in unscaled variables, we see that the solutions will match provided that

$$\frac{R_m}{2}e^{-Z/R_m} = R_0 e^{-1/2} e^{-2(H_2+Z)/(\delta_3 R_m)}, \tag{25}$$

i.e. provided that $\delta_3 = 2$ and

$$H_2 = R_m \log\left(\frac{2e^{-1/2}R_0}{R_m}\right). \tag{26}$$

Recalling that $2\bar{h}R_0^2 = \delta_3$ we deduce that

$$R_0 = \bar{h}^{-1/2}, \tag{27}$$

and so

$$H_2 = R_m \log\left(\frac{2e^{-1/2}}{R_m \bar{h}^{1/2}}\right). \tag{28}$$

Using equations (22) and (28) we deduce that the unknown scaling $\bar{h} \gg 1$ satisfies

$$2\bar{h} \sim \log\left(\frac{8e^{-\gamma}e^{-1/2}}{{R_m}^2 \bar{h}^{1/2}}\right), \tag{29}$$

from which we obtain

$$\bar{h} = -\log R_m, \tag{30}$$

and thus equations (27) and (28) yield

$$R_0 = (-\log R_m)^{-1/2} \tag{31}$$

and

$$H_2 = R_m \log\left(\frac{2e^{-1/2}}{R_m(-\log R_m)^{1/2}}\right). \tag{32}$$

3.5. Solutions for $\hat{R}(R_m, \theta)$ and $\hat{H}(R_m, \theta)$

Having obtained solutions in all three regions and matched them together appropriately we can now construct the complete solution for all values of $\theta \in (0, \pi]$ and, in particular, determine expressions for $\hat{R}(R_m, \theta)$ and $\hat{H}(R_m, \theta)$.

3.5.1. *The case* $\theta \in (0, \pi)$

When $\theta \in (0, \pi)$ region 3 plays no role in the solution and the condition $R_Z = \cot\theta$ is satisfied by the solution in region 1 when $\sinh z_1 = \cot\theta$, i.e. when

$$r_1 = \frac{1}{\sin\theta} \quad \text{at} \quad z_1 = \log\left(\frac{1+\cos\theta}{\sin\theta}\right). \tag{33}$$

Hence

$$\hat{R} = \frac{R_m}{\sin\theta} + o(R_m) \tag{34}$$

and

$$\hat{H} = -R_m \log R_m + R_m \log\left(\frac{4e^{-\gamma}\sin\theta}{1+\cos\theta}\right) + o(R_m). \tag{35}$$

Since $\hat{R} \sim R_m$ as $R_m \to 0$, the result in equation (35) is in exact agreement with the corresponding expression for the height of the meniscus on a cylindrical rod of radius $\hat{R}$ obtained by James [6] in the limit $\hat{R} \to 0$, which can be recovered by using equation (34) to re-write equation (35) in terms of $\hat{R}$.

Equations (34) and (35) hold for all values of $\theta \in (0, \pi)$ and, in particular, are in agreement with those which can be obtained in the limit $\theta \to 0$ by using the familiar ideas of lubrication theory. In this limit the problem can be solved exactly to yield

$$\hat{H} = \theta\frac{K_0(\hat{R})}{K_1(\hat{R})} \tag{36}$$

and taking the limit $\hat{R} \to 0$ of equation (36) we obtain

$$\hat{H} = -\hat{R}\theta \log \hat{R} + \hat{R}\theta \log(2e^{-\gamma}) + o(\hat{R}), \tag{37}$$

in accord with equation (35) in the limit $\theta \to 0$. Note that in the planar case the corresponding analysis yields simply $\hat{H} = \theta$, in agreement with the exact solution available in this case.

3.5.2. *The case $\theta = \pi$*

When $\theta = \pi$ the shape of the free surface is described by the entire universal curve $R = R(Z)$ and so the solution in region 3 is important. In this case $\hat{R} = R_0$ and $\hat{H} = H$ and hence

$$\hat{R} = (-\log R_m)^{-1/2} + o((-\log R_m)^{-1/2}) \tag{38}$$

and

$$\hat{H} = -2R_m \log R_m - \frac{R_m}{2}\log(-\log R_m) + o(R_m \log(-\log R_m)). \tag{39}$$

4. Numerical solution

The numerical solution of equation (1) was performed using a Runge-Kutta-Merson method implemented using NAG routine D02BGF running under UNIX on a SUN SPARCstation 10. The procedure employed to do this was the same as that used by Taylor and Michael [1]. Firstly, H_1 was determined by integrating equation (1) forward from $R = R_m$ at $Z = 0$ for a range of values of H_1 until the boundary condition $\tan^{-1} R_Z \to \pi/2$ as $Z \to H_1^-$ was satisfied to the desired degree of accuracy. Secondly, the values of $\hat{H}$ and $\hat{R}$ corresponding to a particular value of θ were obtained by integrating equation (1) forwards (for $\theta \in (0, \pi/2)$) or backwards (for $\theta \in (\pi/2, \pi]$) from $R = R_m$ at $Z = 0$ until the condition $R_Z = \cot\theta$

Table 1. Comparison between the present numerically calculated ($\hat{H}_N$) and asymptotic ($\hat{H}_A$) results and Sharma's [5] asymptotic ($\hat{H}_A^*$) result for $\hat{H}$ for various values of R_m when $\theta = \pi/18$, $\pi/2$ and $17\pi/18$.

$\theta = \pi/18$					
R_m	$\hat{H}_N/R_m$	$\hat{H}_A^*/R_m$	$\hat{H}_A/R_m$	$(\hat{H}_A^* - \hat{H}_N)/R_m$	$(\hat{H}_A - \hat{H}_N)/R_m$
1	0.14416862	−1.7430989	−1.6271674	−1.8872675	−1.7713360
10^{-1}	0.96225753	0.55948622	0.67541774	−0.40277131	−0.28683979
10^{-2}	2.9869609	2.8620713	2.9780028	−0.1248896	-8.9581×10^{-3}
10^{-3}	5.2807354	5.1646564	5.2805879	−0.1160790	-1.475×10^{-4}
10^{-4}	7.5831751	7.4672415	7.5831730	−0.1159336	-2.1×10^{-6}
10^{-5}	9.8857581	9.7698266	9.8857581	−0.1159315	$< 1 \times 10^{-7}$
10^{-6}	12.188343	12.072412	12.188343	−0.115931	$< 1 \times 10^{-6}$
$\theta = \pi/2$					
R_m	$\hat{H}_N/R_m$	$\hat{H}_A^*/R_m$	$\hat{H}_A/R_m$	$(\hat{H}_A^* - \hat{H}_N)/R_m$	$(\hat{H}_A - \hat{H}_N)/R_m$
1	0.99702014	0.69314718	0.80907870	−0.30387296	−0.18794144
10^{-1}	3.1114615	2.9957323	3.1116638	−0.1157292	2.023×10^{-4}
10^{-2}	5.4141911	5.2983174	5.4142489	−0.1158737	5.78×10^{-5}
10^{-3}	7.7168328	7.6009025	7.7168340	−0.1159303	1.2×10^{-6}
10^{-4}	10.019419	9.9034876	10.019419	−0.115931	$< 1 \times 10^{-6}$
10^{-5}	12.322004	12.206073	12.322004	−0.115931	$< 1 \times 10^{-6}$
10^{-6}	14.624589	14.508658	14.624589	−0.115931	$< 1 \times 10^{-6}$
$\theta = 17\pi/18$					
R_m	$\hat{H}_N/R_m$	$\hat{H}_A^*/R_m$	$\hat{H}_A/R_m$	$(\hat{H}_A^* - \hat{H}_N)/R_m$	$(\hat{H}_A - \hat{H}_N)/R_m$
1	1.4950548	3.1293932	3.2453248	1.6343384	1.7502700
10^{-1}	4.9760776	5.4319783	5.5479098	0.4559007	0.5718322
10^{-2}	7.8327229	7.7345634	7.8504949	−0.0981595	0.0177720
10^{-3}	10.152840	10.037149	10.153080	−0.115691	2.40×10^{-4}
10^{-4}	12.455662	12.339734	12.455665	−0.115928	3×10^{-6}
10^{-5}	14.758250	14.642319	14.758250	−0.115931	$< 1 \times 10^{-6}$
10^{-6}	17.060835	16.944904	17.060835	−0.115931	$< 1 \times 10^{-6}$

was satisfied to the desired degree of accuracy. Figure 2 gives typical numerically calculated curves $R = R(Z)$ for a range of values of R_m.

Tables 1 and 2 show comparisons between numerically calculated values of $\hat{R}$ and $\hat{H}$, Sharma's [5] asymptotic result for $\hat{H}$ given by equation (42), and the present asymptotic results for $\hat{R}$ and $\hat{H}$ given by equations (34) and (35) respectively for various values of R_m when $\theta = \pi/18$, $\pi/2$ and $17\pi/18$. These results clearly demonstrate both the excellent agreement between the present numerical and asymptotic results and the $O(R_m)$ error in Sharma's [5] prediction for $\hat{H}$. In particular, the results displayed in Table 1 confirm that the next term in the expansion of $\hat{H}$ is indeed $o(R_m)$ and suggests it may in fact be $O({R_m}^2)$. Similarly, the values displayed in Table 2 confirm that the next term in the expansion of $\hat{R}$ is indeed $o(R_m)$ and suggest it may also be $O({R_m}^2)$.

Table 2. Comparison between the present numerically calculated ($\hat{R}_N$) and asymptotic ($\hat{R}_A$) results for $\hat{R}$ for various values of R_m when $\theta = \pi/18$ and $17\pi/18$. Note that in the case $\theta = \pi/2$ the relationship $\hat{R} = R_m$ is exact.

$\theta = \pi/18$			
R_m	$\hat{R}_N/R_m$	$\hat{R}_A/R_m$	$(\hat{R}_A - \hat{R}_N)/R_m$
1	2.1927909	5.7587705	3.5659796
10^{-1}	4.8614272	5.7587705	0.8973433
10^{-2}	5.7271346	5.7587705	0.0316359
10^{-3}	5.7582380	5.7587705	5.325×10^{-4}
10^{-4}	5.7587630	5.7587705	7.5×10^{-6}
10^{-5}	5.7587704	5.7587705	1×10^{-7}
10^{-6}	5.7587705	5.7587705	$< 1 \times 10^{-7}$
$\theta = 17\pi/18$			
R_m	$\hat{R}_N/R_m$	$\hat{R}_A/R_m$	$(\hat{R}_A - \hat{R}_N)/R_m$
1	1.4433456	5.7587705	4.3154249
10^{-1}	3.8862262	5.7587705	1.8725443
10^{-2}	5.6921680	5.7587705	0.0666025
10^{-3}	5.7578740	5.7587705	8.965×10^{-4}
10^{-4}	5.7587594	5.7587705	1.11×10^{-5}
10^{-5}	5.7587704	5.7587705	1×10^{-7}
10^{-6}	5.7587705	5.7587705	$< 1 \times 10^{-7}$

Table 3. Comparison between the present numerically calculated (H_{2N}) and asymptotic (H_{2A}) results for H_2 for various values of R_m when $\theta = \pi$.

$\theta = \pi$			
R_m	H_{2N}/R_m	H_{2A}/R_m	$(H_{2A} - H_{2N})/R_m$
1	0.50766064		
10^{-1}	2.0655896	1.8855689	−0.1800207
10^{-2}	4.0543630	3.8415804	−0.2127826
10^{-3}	6.1556021	5.9414329	−0.2141692
10^{-4}	8.3130924	8.1001770	−0.2129154
10^{-5}	10.502625	10.291190	−0.211435
10^{-6}	12.712681	12.502615	−0.210066

Tables 3 and 4 show comparisons between numerically calculated values of $\hat{R}$ and H_2 and the present asymptotic results given by equation (38) and

$$H_2 = -R_m \log R_m - \frac{R_m}{2} \log(-\log R_m) + o(R_m \log(-\log R_m)), \tag{40}$$

for various values of R_m when $\theta = \pi$. These results again demonstrate the excellent agreement between the present numerical and asymptotic results. In particular, they confirm that the next term in the expansion of H_2 is indeed $o(R_m \log(-\log R_m))$ while the next term in the expansion of $\hat{R}$ is indeed $o((-\log R_m)^{-1/2})$.

Table 4. Comparison between the present numerically calculated ($\hat{R}_N$) and asymptotic ($\hat{R}_A$) results for $\hat{R}$ for various values of R_m when $\theta = \pi$.

$\theta = \pi$			
R_m	$\hat{R}_N$	$\hat{R}_A$	$\hat{R}_A - \hat{R}_N$
1	1.5547		
10^{-1}	0.6439	0.6590	0.0151
10^{-2}	0.4660	0.4660	$< 1 \times 10^{-4}$
10^{-3}	0.3832	0.3805	−0.0027
10^{-4}	0.3326	0.3295	−0.0031
10^{-5}	0.2977	0.2947	−0.0030
10^{-6}	0.2717	0.2690	−0.0027

5. Comparison with earlier work

Sykes [4] treated the present problem when $\theta \in (0, \pi)$ by making the ad hoc assumption that the zero-gravity solution appropriate in region 1 satisfies $R(H_1) = 1 + \hat{R}$. Imposing this condition and exploiting the fact that $\hat{H}/(\hat{R}\sin\theta) \gg 1$ she obtained the approximate expression

$$\hat{H} = \hat{R}\sin\theta \log\left(\frac{2(1+\hat{R})}{(1+\cos\theta)\hat{R}}\right), \tag{41}$$

which, by comparison with equations (34) and (35), we can now see is correct only at leading order in the limit $R_m \to 0$.

Subsequently Sharma [5] addressed the present problem when $\theta \in (0, \pi)$ in the limit $R_m \to 0$. His solution in region 1 agrees with the present one, but in region 2 he incorrectly suggested that the leading order problem was simply that corresponding to a planar hole. As a consequence he was unable to match the solutions correctly and the ad hoc "patching" he used instead amounts to requiring that the zero-gravity solution appropriate in region 1 satisfies $R(H_1) = 1$. Imposing this condition and exploiting the fact that $\hat{H}/R_m \gg 1$ he obtained the approximate expression

$$\hat{H} = R_m \log\left(\frac{2\sin\theta}{(1+\cos\theta)R_m}\right), \tag{42}$$

which we can now see is also correct only at leading order in the limit $R_m \to 0$. The present numerical results for $\hat{H}$ given in Table 1 extend and correct the corresponding results given by Sharma [5, Table 1].

Inspection of the present asymptotic solution shows that the solution in region 1 satisfies $R(H_1) = 2e^{-\gamma} + o(1)$, where $2e^{-\gamma} \simeq 1.122918967$, and so had either of the above authors used this condition instead they would have obtained the present expression for $\hat{H}$, which is accurate to $O(R_m)$ in the limit $R_m \to 0$.

Recently Sykes *et al.* [10] reported a series of experiments in which holes of various sizes were made in layers of two different fluids lying on a horizontal substrate. Following Sykes *et al.* [10] in Fig. 3 we plot the dimensional thickness of the layer, $\hat{H}^*$, as a function of dimensional hole radius, $\hat{R}^*$, and show the comparison between Sykes *et al.*'s [10] experimental results,

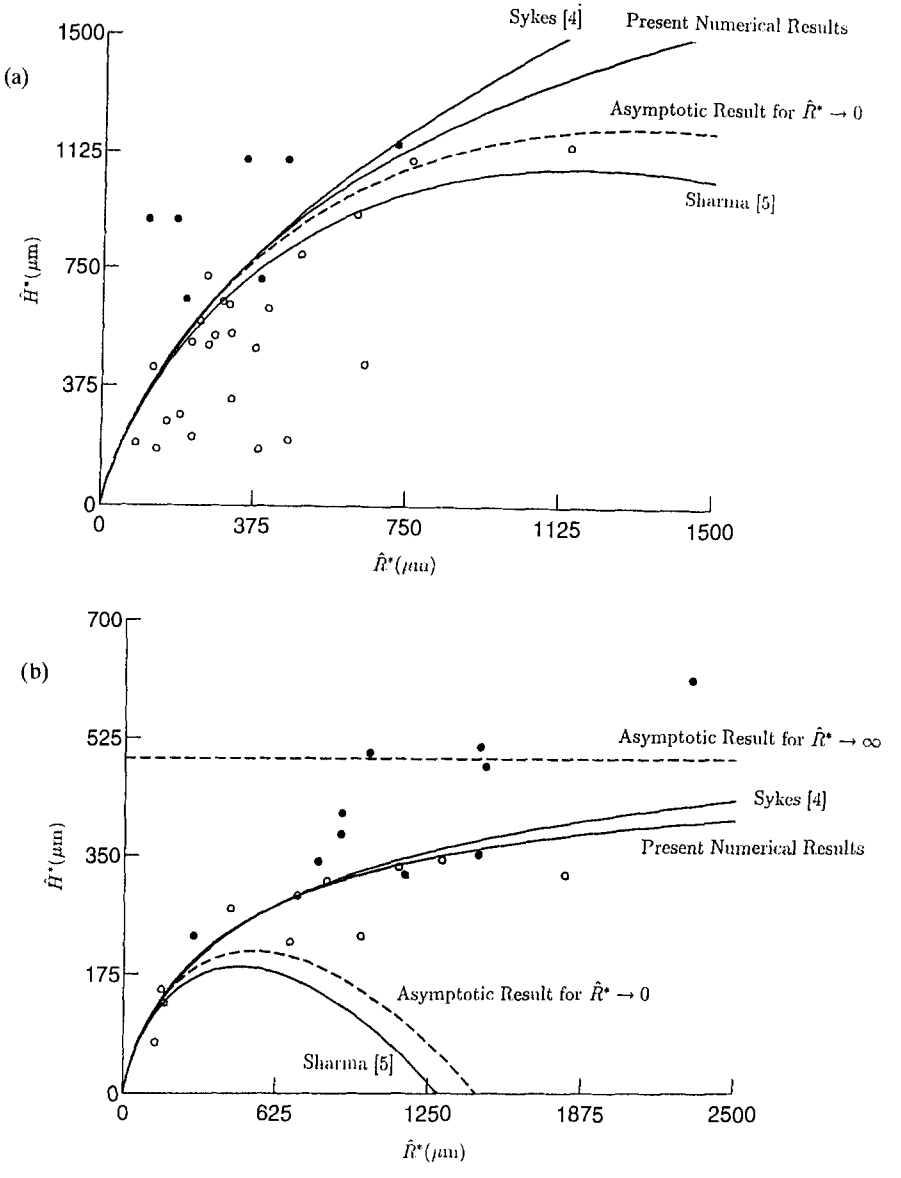

Fig. 3. Dimensional thickness of the layer $\hat{H}^*$ as a function of dimensional hole radius $\hat{R}^*$ showing the comparison between the experimental data of Sykes *et al.* [10] and theory for (a) glycerol and (b) di-iodomethane. The experimental points corresponding to holes which closed are denoted by solid circles (•) while those which opened are denoted by open circles (o). The curves denote the values of $\hat{H}^*$ obtained from the present numerical calculations, the approximate expressions of Sykes [4] (equation (41)) and Sharma [5] (equation (42)) and the asymptotic results for both large and small values of $\hat{R}^*$. Note that in case (a) the asymptotic value of $\hat{H}^*$ for large $\hat{R}^*$ is approximately 2460 μm and hence this curve does not appear on the figure.

the values obtained from the present numerical calculations, the approximate expressions of Sykes [4] (equation (41)) and Sharma [5] (equation (42)) and the asymptotic results for both large and small values of $\hat{R}^*$. Figure 3(a) shows the results for glycerol (for which $l_c = 2260$ μm) calculated using $\theta = 66^o$, while Fig. 3(b) shows the results for di-iodomethane ($l_c = 1240$ μm) calculated using $\theta = 23^o$. In particular, Fig. 3 shows that the division between holes which open and holes which close is in good agreement with the numerically calculated value

of $\hat{H}^*$. Figure 3 also shows that, as we expect, the asymptotic theory for small holes is a good approximation to the numerical solution provided that $\hat{R}^* \ll l_c$. Sykes' [4] approximate expression for $\hat{H}^*$ was also derived on the assumption that the radius of the hole was small; however, despite the fact that it is correct only at leading order for small holes and does not have the correct asymptotic behaviour for large holes, it evidently agrees quite well with the numerically calculated solution over the range of values of $\hat{R}^*$ shown.

6. The planar problem

The equivalent planar problem is given by omitting the azimuthal curvature term from the Young-Laplace equation (??) but is otherwise identical provided we now interpret R as a cartesian coordinate. It is interesting to understand why the present asymptotic approach does not work for the planar problem. Adopting the same notation as for the axisymmetric case the solution near $Z = 0$ is now simply $r_1(z_1) = 1$ which cannot in general be matched to the solution $z_2 = B_2 e^{-r_2}$ near $Z = H_1$ or $z_3 = (r_3 - 1)^2/2$ near $Z = -H_2$. Of course, as Lamb [3, §127] describes, in the planar case the full problem can be solved exactly to yield $\hat{H} = 2\sin(\theta/2)$ and so, unlike in the axisymmetric case, solutions with $\hat{H} \ll 1$ are possible only when $\theta \ll 1$, in which case $\hat{H} = \theta + O(\theta^3)$.

7. Conclusions

In this paper we have obtained the description of axisymmetric equilibrium holes in thin fluid layers lying on a horizontal substrate under the influence of surface tension and gravity effects in the asymptotic limit when the radius of the hole is small. In particular, we have shown that the asymptotic expressions for the radius of the hole at the substrate, $\hat{R}$, and the thickness of the layer far from the hole, $\hat{H}$, in the limit $R_m \to 0$ are given by equations (??) and (??) when $\theta \in (0, \pi)$ and by equations (??) and (??) when $\theta = \pi$. The correctness of these expressions was confirmed by comparison with numerical solutions to the full problem. In the light of the present study we were able to highlight shortcomings in the earlier work of Sykes [4] and Sharma [5] and, in particular, show that their predictions for $\hat{H}$ when $\theta \in (0, \pi)$ are correct only at leading order in the limit $R_m \to 0$.

References

1. G. I. Taylor and D. H. Michael, On making holes in a sheet of fluid, *J. Fluid Mech.* 58 (1973) 625-639.
2. S. K. Wilson and E. L. Terrill, The dynamics of planar and axisymmetric holes in thin fluid layers, *University of Strathclyde Department of Mathematics Research Report* 14 (1995).
3. H. Lamb, *Statics* (2nd Edition), Cambridge University Press (1924).
4. C. Sykes, Transition d'immersion de défauts non mouillants (Immersion transition of non wetting defects), *C. R. Acad. Sci. Paris II* 313 (1991) 607-612. (In French with extended summary in English.)
5. A. Sharma, Disintegration of macroscopic fluid sheets on substrates: a singular perturbation approach, *J. Coll. Int. Sci.* 156 (1993) 96-103.
6. D. F. James, The meniscus on the outside of a small circular cylinder, *J. Fluid Mech.* 63 (1974) 657-664.
7. L. L. Lo, The meniscus on a needle - a lesson in matching, *J. Fluid Mech.* 132 (1983) 65-78.
8. C. Huh and L. E. Scriven, Shapes of axisymmetric fluid interfaces of unbounded extent, *J. Coll. Int. Sci.* 30 (1969) 323-337.
9. S. B. G. O'Brien, On the shape of small sessile and pendant drops by singular perturbation techniques, *J. Fluid Mech.* 233 (1991) 519-537.
10. C. Sykes, C. Andrieu, V. Détappe and S. Deniau, Critical radius of holes in liquid coating, *J. Phys. III France* 4 (1994) 775-781.